SANDIA REPORT

SAND2005-5510
Unlimited Release
Printed September 2005

A Novel Polar Format Algorithm for SAR Images Utilizing Post Azimuth Transform Interpolation

Grant D. Martin, Armin W. Doerry, and Michael W. Holzrichter

Prepared by
Sandia National Laboratories
Albuquerque, New Mexico 87185 and Livermore, California 94550

Sandia is a multiprogram laboratory operated by Sandia Corporation, a Lockheed Martin Company, for the United States Department of Energy under Contract DE-AC04-94AL85000.

Issued by Sandia National Laboratories, operated for the United States Department of Energy by Sandia Corporation.

Available to DOE and DOE contractors from
U.S. Department of Energy
Office of Scientific and Technical Information
P.O. Box 62
Oak Ridge, TN 37831

Telephone: (865)576-8401
Facsimile: (865)576-5728
E-Mail: reports@adonis.osti.gov
Online ordering: http://www.doe.gov/bridge

Available to the public from
U.S. Department of Commerce
National Technical Information Service
5285 Port Royal Rd
Springfield, VA 22161

Telephone: (800)553-6847
Facsimile: (703)605-6900
E-Mail: orders@ntis.fedworld.gov
Online order: http://www.ntis.gov/ordering.htm

SAND2005-5510
Unlimited Release
Printed September 2005

A Novel Polar Format Algorithm for SAR Images Utilizing Post Azimuth Transform Interpolation

Grant D. Martin, Michael W. Holzrichter
Embedded Radar Processing Department

Armin W. Doerry
SAR Applications Department

Sandia National Laboratories
PO Box 5800
Albuquerque, NM 87185-1330

ABSTRACT

SAR phase history data represents a polar array in the Fourier space of a scene being imaged. Polar Format processing is about reformatting the collected SAR data to a Cartesian data location array for efficient processing and image formation. In a real-time system, this reformatting or "re-gridding" operation is the most processing intensive, consuming the majority of the processing time; it also is a source of error in the final image. Therefore, any effort to reduce processing time while not degrading image quality is valued. What is proposed in this document is a new way of implementing real-time polar-format processing through a variation on the traditional interpolation / 2-D Fast Fourier Transform (FFT) algorithm. The proposed change is based upon the frequency scaling property of the Fourier Transform, which allows a post azimuth FFT interpolation. A post azimuth processing interpolation provides overall benefits to image quality and potentially more efficient implementation of the polar format image formation process.

ACKNOWLEDGEMENTS

This work was funded by the US DOE Office of Nonproliferation & National Security (NNSA), Office of Research and Development, Proliferation Detection Program Office (NA-22), under the Advanced Radar System (ARS) project.

Sandia is a multi-program laboratory operated by Sandia Corporation, a Lockheed Martin Company, for the United States Department of Energy under Contract DE-AC04-94AL85000.

CONTENTS

Foreword

Sandia developed Synthetic Aperture Radars (SAR's) produce quality, high-resolution images in real-time for several operating modes. These SAR systems continue to push the envelope for the technology such that real-time processing demands are becoming increasingly difficult. Therefore, any effort to optimize the image formation process without sacrificing the quality of images is necessary.

The algorithm described within this document resulted from an effort to reduce processing time without sacrificing image quality. The recently developed Sandia SAR platform MiniSAR is capable of producing images with this technique, and has demonstrated this algorithm during flight tests.

1. Introduction & Background

Synthetic Aperture Radar (SAR) images a scene by sampling and then coherently processing RF energy returns along the radar flight path. These energy returns are the reflections from a space-varying function (scene) and may be processed to represent samples in the Fourier space of the scene. In other words, the Fourier space of the scene is the Fourier Transform of the 3-D complex reflectivity of the scene being imaged. Thus, with the typical assumption of a flat scene, image formation can be accomplished via a 2-D Fourier Transform. Residual errors in the data model will, however, effectively limit the region within the image that exhibits optimum focusing. When a large scene is imaged at a fine resolution, a simple 2-D Fourier Transform (linear range-Doppler processing) is inadequate due to target Motion Through Resolution Cells (MTRC) [1]. In order to alleviate the image smearing caused by MTRC, Walker developed a recording technique known as polar format processing [2]. Polar format processing was originally accomplished optically, where the SAR data or phase histories were recorded on a disk-shaped rotating film and lenses were used for the Fourier Transform. With later developments in tomography, and eventually digital tomography, Munson et al [3], showed that under the constraint of a planar wavefront approximation, the raw data that embodies the Fourier representation of the image are samples distributed on a polar grid. However, with the move from optical systems to digital systems for recording raw phase history data, polar format processing is no longer about rotating films and 2-D Fourier Transforms with lenses, but about the need to get the data to a Cartesian grid array for efficient digital processing and image formation of the collected SAR data.

In a real-time system, the polar-to-rectangular “re-gridding” operation is the most processing intensive, consuming the majority of the processing time. Typically, 2-D data interpolation techniques are used to reformat the data, although it is possible to manipulate radar hardware to vary pulse-to-pulse waveform and sampling parameters to considerably simplify the subsequent resampling, and limit it to a 1-D operation, thereby helping reduce some of the processing time required. Sandia radar systems are capable of this and often collect data on a trapezoidal grid that is both uniformly spaced in the range direction; and per each row, uniformly spaced in the azimuth direction. This trapezoidal grid leads to a reconstruction algorithm where the simplified procedure is to interpolate each row in the azimuth direction to the Cartesian grid, so that a 2-D FFT can be used to generate the image. However, this technique exhibits shortcomings in that first, the interpolation kernel to produce good results on complex data is difficult to create without leaving artifacts in the image; and second, the number of interpolations required is large, considering that the number image pixels will often only be a fraction of the total number of points in the phase history data. Even though this interpolation procedure can be efficient, it is still often the dominating factor in the processing time required for the algorithm as well as a source of error in the final image.

A second, alternative reconstruction algorithm for the trapezoidal grid uses the Fractional Fourier Transform or "Chirp-Z" along the azimuth direction, followed by a FFT in the range direction [9]. This method produces excellent results when implemented as a fast-convolution. However, while avoiding the errors of interpolation, it is often even less computationally efficient when compared to other methods that give similar quality results. Therefore, any effort to reduce processing time while not degrading image quality is valued.

What is proposed in this document is a new way of implementing real-time polar-format processing through a variation on the traditional interpolation/2-D FFT algorithm. Therefore, in order to better understand how this method works, it is necessary to first describe a standard SAR system phase history recording and also the polar format image formation algorithm. Following the discussion of a standard SAR system, the proposed methods and improvements will be discussed.

SAR Data Collection – Gathering the Fourier Space of a Scene (Phase Histories)

Consider the 3-D radar geometry of figure 1, where

$\boldsymbol{s}$ = the spatial location of a point target, with coordinates (s_x, s_y, s_z),
$\boldsymbol{r_c}$ = the location of the radar, with coordinates (r_x, r_y, r_z), and
$\boldsymbol{r_s} = \boldsymbol{r_c} - \boldsymbol{s}$ = relation of radar location to the point target location.

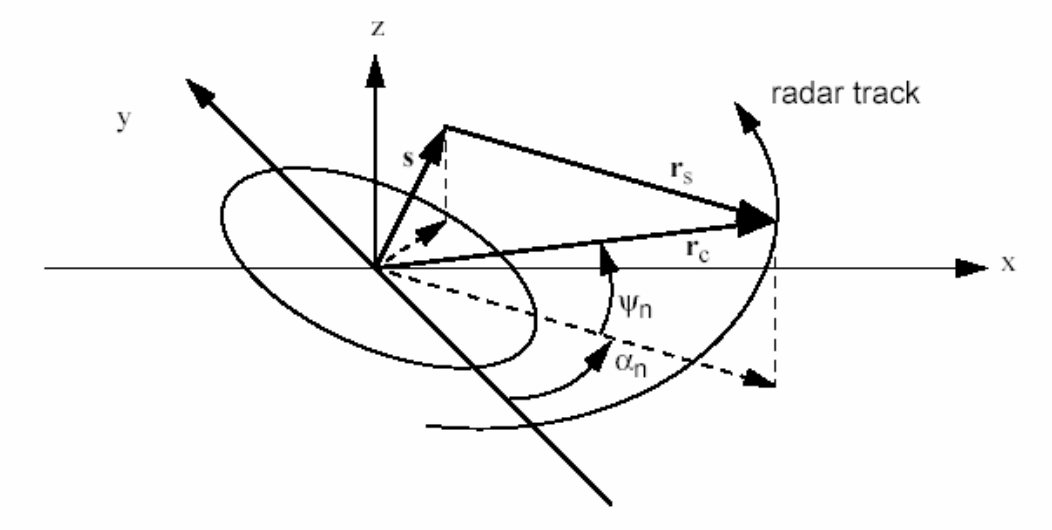

Figure 1: Radar Geometry of a 3-D Scene

Angles α_n and ψ_n denote the orientation of the vector $\boldsymbol{r_c}$. Subscripts n denote parameters for the n^{th} indexed pulse position along the flight path. Note that conventional SAR presumes that $\boldsymbol{s}$ is fixed, but $\boldsymbol{r_c}$ varies with n.

Also, consider a linear frequency modulated (LFM) "chirp" pulse as the transmitted waveform. This pulse is common in high resolution SAR imaging and is represented by the following equation:

$$x_T(t) = A_T\, rect\left(\frac{t}{T}\right)\cos\left(\omega \cdot t + \frac{\gamma}{2}t^2\right). \qquad (1)$$

where

ω = center frequency of the transmitted pulse,
γ = chirp rate of the transmitted pulse,
A_T = amplitude of the transmitted pulse,
T = duration of transmitted pulse, and

$$rect(x) = \begin{cases} 1 & |x| < 1/2, \\ 0 & otherwise, \end{cases} .$$

While traversing the radar track of figure 1, the SAR will receive an echo from the target at location ***s,*** which will be a scaled and time delayed version of the transmitted signal, namely

$$X_R(t) =$$

$$\frac{A_R}{A_T}\sigma(\mathbf{s})X_T(t-t_s) = A_R\sigma(\mathbf{s})rect\left(\frac{t-t_s}{T}\right)\cos\left(\omega\cdot(t-t_s) + \frac{\gamma}{2}(t-t_s)^2\right) \qquad (2)$$

where

A_R is the nominal amplitude of the received echo, and
$\sigma(\boldsymbol{s})$ is the reflectivity of the target at ***s***.

The echo delay time with respect to the target depends on the distance to the target and the speed of wave propagation, and is

$$t_s = \frac{2}{c}|\mathbf{r_s}|. \qquad (3)$$

The echo delay time of the scene center is given by

$$t_c = \frac{2}{c}|\mathbf{r_c}|. \qquad (4)$$

Note that these times will generally both vary with *n*. De-chirping this (stretch processing)[4], using quadrature demodulation, and ignoring a minor phase term often

referred to as the residual video phase error (RVPE), yields a signal of the approximate form

$$X_V(t') \approx A_R \sigma(s) rect\left(\frac{t'}{T}\right) \exp\ j\{[\omega + \gamma t'](t_c - t_s)\}, \quad (5)$$

where $t' = t - t_c$, which varies over the interval $-T/2$ to $T/2$. These are common operations and assumptions for polar format processing. The RVPE in any case is easily mitigated with some pre-processing, often called deskewing [5, 6]. Now, when an Analog to Digital converter (ADC) is used to sample at times $t' = iT_s$, where i is the sample index and T_s is the ADC sample spacing, the sampled video signal becomes

$$X_V(t') \approx A_R \sigma(s) \exp\ j\{[\omega + \gamma \cdot T_S i](t_c - t_s)\}. \quad (6)$$

Note that the quantity $[\omega + \gamma \cdot T_S i]$ is an instantaneous frequency expression. Also, the time difference quantity $t_c - t_s$ is related to range, which includes target height and radar height, and can be expanded to

$$(t_c - t_s) \approx \frac{2}{c}\left(s_x \cos\psi_n \sin\alpha_n - s_y \cos\psi_n \cos\alpha_n + s_z \sin\psi_n\right). \quad (7)$$

By allowing frequency, chirp rate, and ADC sampling to vary with pulse index n, the video signal may be expanded into wavenumber components as

$$X_V(i,n) \approx A_R \sigma(s) \exp\ j\{k_x(i,n)s_x + k_y(i,n)s_y + k_z(i,n)s_z\}, \quad (8)$$

where

$$k_x(i,n) = \frac{2}{c}[\omega_n + \gamma_n T_{s,n} i]\cos\psi_n \sin\alpha_n, \quad (9)$$

$$k_y(i,n) = -\frac{2}{c}[\omega_n + \gamma_n T_{s,n} i]\cos\psi_n \cos\alpha_n, \quad (10)$$

$$k_z(i,n) = \frac{2}{c}[\omega_n + \gamma_n T_{s,n} i]\sin\psi_n \quad (11)$$

These wavenumber combinations define coordinates in the Fourier space of the 3-D scene. That is, each individual combination of index i and index n defines a unique wavenumber coordinate, that in turn defines a specific point in the Fourier space of the scene. Consequently, a specific phase history data sample (specific sample from a specific pulse) defines the complex value of a specific location in the Fourier space of the scene. That location is given in spherical coordinates as a distance of $\frac{2}{c} \cdot [\omega_n + \gamma_n T_{s,n} i]$ from the origin, an angle from the negative k_y axis of α_n, and an elevation of ψ_n from the (k_x, k_y) plane (see figure 2).

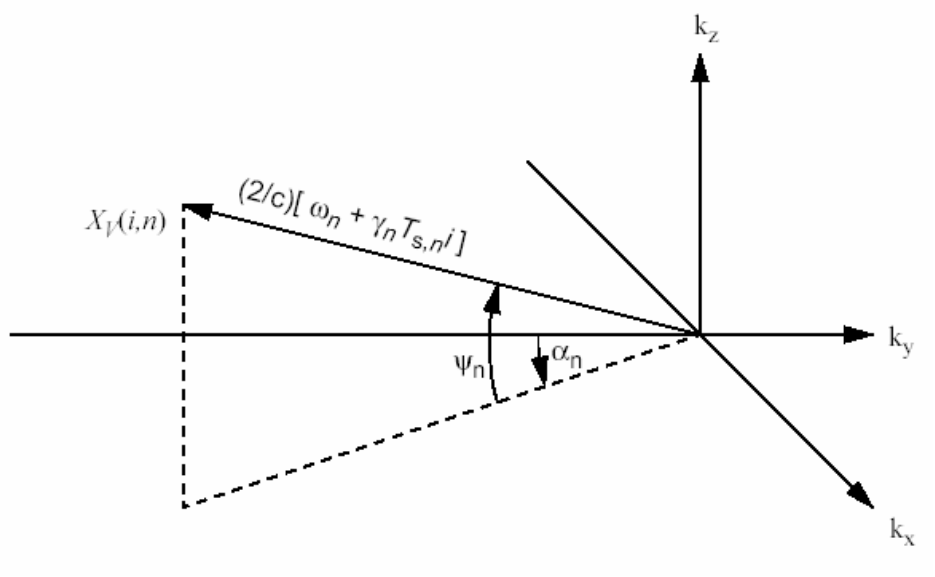

Figure 2: Location in 3-D Fourier space of a single phase history data sample

Similarly, a collection of phase histories defines a set of samples in the Fourier space of the scene. Data collected with constant waveform parameters, and at a constant elevation angle describes a conical polar wedge, and is illustrated in figure 3.

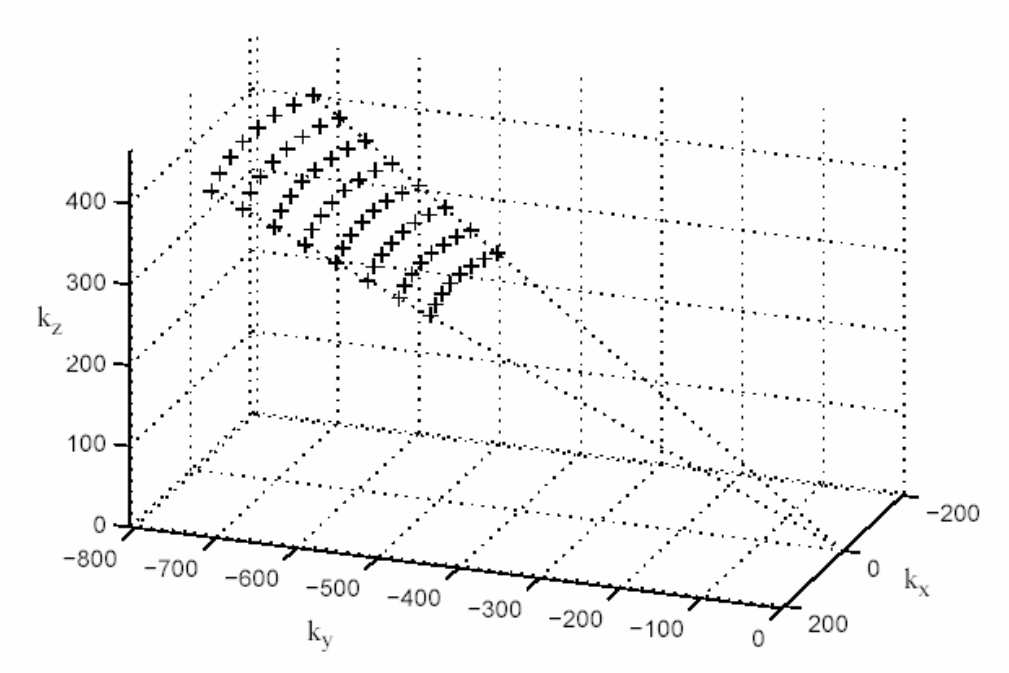

Figure 3: Location in 3-D Fourier space of a phase history data set, from multiple pulses and multiple ADC samples within any pulse.

With the typical assumption of a flat scene surface ($s_z = 0$), the Fourier data is unchanged across k_z and can be projected onto the $k_z = 0$ plane. (see figure 4).

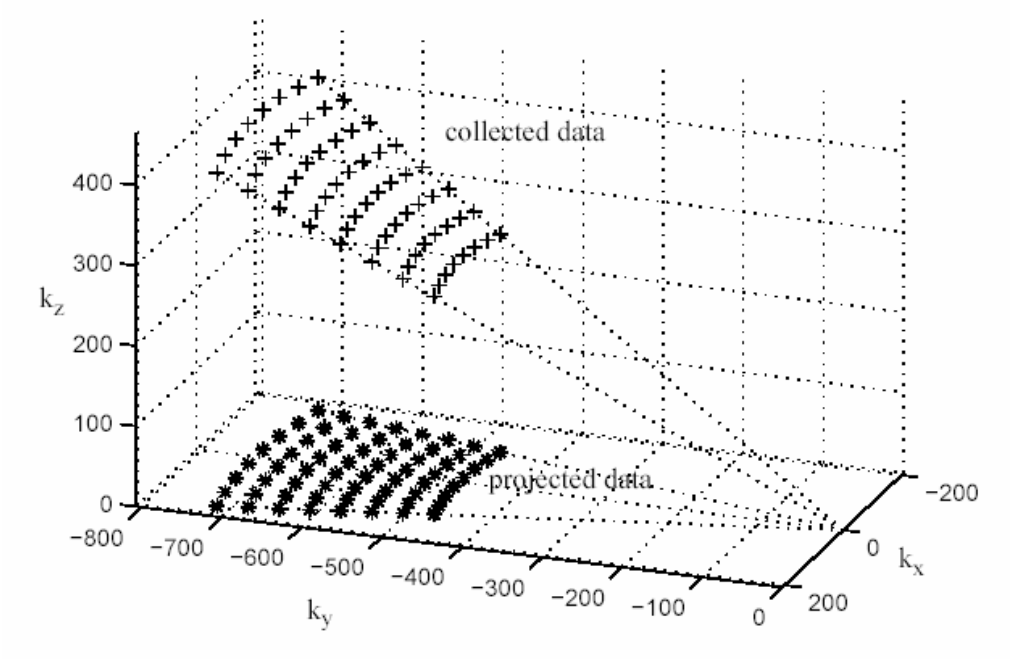

Figure 4: Fourier space locations of a collected phase history data set, and their projection onto the kz = 0 plane.

The projected data is now 2-D, and can be treated as such for transformation to an image of the 3-D scene. The new phase history model for the projected data has become

$$X_V(i,n) \approx A_R \sigma(s) \exp\, j\{k_x(i,n)s_x + k_y(i,n)s_y\} \qquad (12)$$

where,

$$k_x(i,n) = \frac{2}{c}\left[\omega_n + \gamma_n T_{s,n} i\right] \cos\psi_n \sin\alpha_n, \qquad (13)$$

$$k_y(i,n) = -\frac{2}{c}\left[\omega_n + \gamma_n T_{s,n} i\right] \cos\psi_n \cos\alpha_n. \qquad (14)$$

Polar Format Processing

As can be seen from figure 4, the projected data are samples on a polar wedge in the Fourier space of the scene. Unfortunately there are not any efficient algorithms for the direct calculation of the 2-D Discrete Polar Fourier Transform. Also, for display of the image on a CRT monitor or LCD monitor, a polar raster is not readily available. Therefore, it is necessary to perform a polar-to-rectangular resampling in order to use the efficiency of the 2-D FFT algorithm and properly display the formed image.

Various methods exist for transforming data from a polar grid to a rectangular grid, many of which use a 2-D interpolation, but this is computationally inefficient, just like the method of a direct polar Fourier Transform. Therefore, the polar format algorithm uses separability to perform a one dimensional interpolation in the radial direction prior to a one dimensional interpolation in the k_x (azimuth) direction. This method of interpolation is called the keystone, or trapezoidal grid technique [5]. Prior to range interpolation, the projected phase history samples are on a 2-D polar wedge as can be seen by the squares in figure 5. Range interpolation along the radial lines of figure 5 produces a result depicted by the * markers.

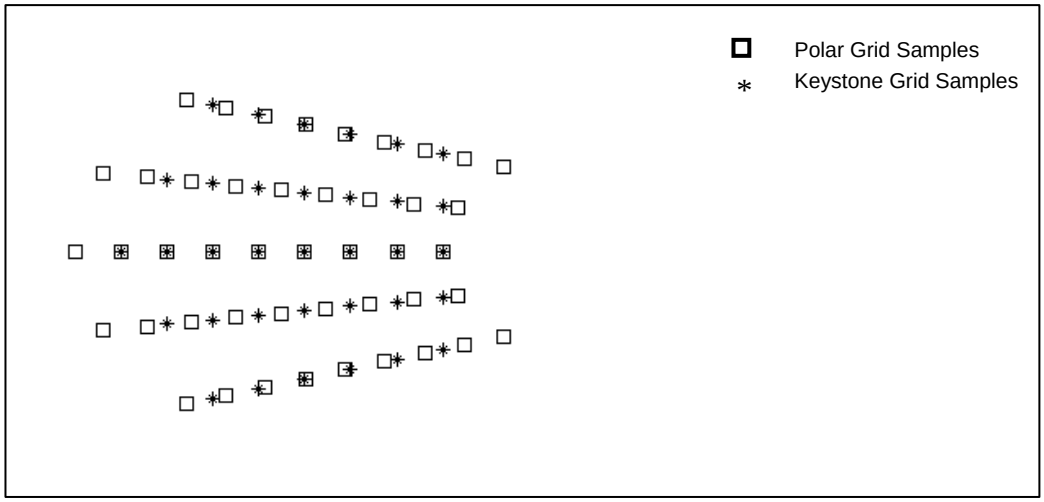

Figure 5: Range Interpolation to Keystone Grid. The original data locations are the squares and the new data locations are denoted with stars.

The range interpolation is performed in the radial direction with the purpose of causing $k_y(i,n)$ to not vary with pulse index n. Consequently, we sample to a new index i' and effect the substitution

$$k_y(i,n) \rightarrow k_y(i',0) = k_y(i') = \frac{2}{c}\left[\omega_0 + \gamma_0 T_{s,0} i'\right]\cos\psi_0 \qquad (15)$$

This implies that we select new sample positions such that

$$\left[\omega_n + \gamma_n T_{s,n} i\right]\cos\psi_n \cos\alpha_n = \left[\omega_0 + \gamma_0 T_{s,0} i'\right]\cos\psi_0 . \qquad (16)$$

A byproduct is that we also effect

$$k_x(i,n) \rightarrow k_x(i',n) = \frac{2}{c}\left[\omega_o + \gamma_o T_{s,o} i'\right]\cos\psi_0 \tan\alpha_n \qquad (17)$$

The next step in the polar format process is a one dimensional interpolation of the new keystone samples in the azimuth direction. Figure 6 shows the keystone samples, as well as the final rectangular grid that the azimuth interpolation produces. This interpolation, analogous to the radial interpolation, removes the dependence of *i'* from k_x**.** The interpolation to be performed in the k_x direction will now modify $k_x(i',n)$ such that

$$k_x(i',n) \rightarrow k_x(n') \qquad (18)$$

This is accomplished by letting

$$\left[\omega_o + \gamma_o T_{s,o} i'\right] \tan\alpha_n = \omega_0 d\alpha \cdot n' \qquad (19)$$

Note that typically the range of *n'* is limited such that the rectangular grid is inscribed within the trapezoidal aperture (see Figure 6).

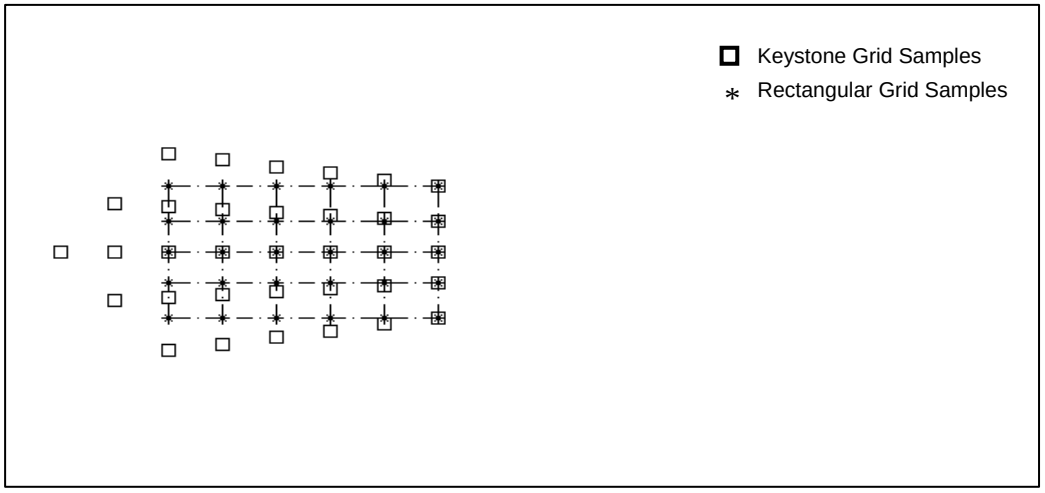

Figure 6: Azimuth Interpolation from keystone samples with final rectangular grid over-lay

By performing interpolation in the manner described, the phase history data will be samples on a rectangular grid, where now a simple 2-D FFT can transform the data for image formation. This completes the process of digital polar format processing.

Several observations are worth noting. First, in practical scenarios, azimuth interpolation is treated in a similar manner to that of the range dimension interpolation [5, 6]. However, upon inspection of the inscribed rectangular grid in Figure 6 it is clear that the interpolation along each column of samples operates on data that is not necessarily linearly spaced. Often in practice the data are sampled at positions where unit increments in index *n* represent constant angular increments in α_n. It is generally assumed that commonly used simple interpolation schemes do not produce unreasonable errors in spite

of non-uniform sample spacing because the angular extent of the phase history is often only a few degrees. However, due to the azimuth sample separation increasing per each range column, optimal filter design for interpolation must accommodate the sample spacing change to mitigate error. A second observation to note is that an ideal reconstruction filter is not realizable. This means that in filter design many tradeoffs are necessary between maintaining flat passbands, high transition slope, and good stopband rejection. Longer filters for resampling will give better interpolation results, but will add additional computational burden. Alternatively, small interpolation filters will produce errors that will be compounded through each step of the polar format algorithm. Lastly, it is well known that the span of the phase history determines the resolution of the final image, while the density of points determines the spatial extent of the scene in the image. Since the Cartesian grid used for image formation is usually an inscribed rectangle of the phase history data (at least in common applications), the final image is not using the complete available information in regards to resolution. This essentially throws out data and causes a slight otherwise unnecessary blurring in the final image.

It has already been reported in the literature how the range interpolation can be equivalently accomplished by varying pulse-to-pulse waveform parameters and/or digital sampling parameters. [7, 8, 10, 12] Proper manipulation of these obviates the need for an overt range interpolation step by placing the raw data samples onto their correct Fourier domain locations to begin with. This in and of itself is not a new idea [7, 8], and is a data format used by Lawton [9]. The range formatted phase history data is now in a trapezoidal form and for traditional polar format image processing needs only to be interpolated along each azimuth line prior to a 2-D FFT to complete the process.

Proper control of pulse timing can force azimuth samples to be linearly spaced as well. This is accomplished by collecting data at angles such that $\tan\alpha_n = \delta\alpha\, n$.

This report details modifications and improvements to the basic algorithm that enhance efficiency and performance without degrading the quality of the resulting image.

2. Overview & Summary

The proposed new method of polar format processing begins with phase history data properly aligned in range and linearly spaced in azimuth, on a trapezoidal grid. Recall that a radar can be designed and operated to collect raw data directly with these characteristics by waveform and timing manipulations. Subsequently, by recognizing the scaling property of the Fourier Transform, the new method performs interpolation after the FFT in the azimuth direction, instead of before the FFT. Once the interpolation is complete, a range dimension FFT is performed to complete image formation and the polar format processing algorithm.

This new method will provide tangible benefits to image quality and efficiency as well as overcome some of the deficiencies in the more traditional versions of polar format processing.

1. Since the transform happens prior to interpolation, this new technique uses the entire frequency space of the data and is not limited to the region of an inscribed rectangle, thereby offering slightly improved resolution.

2. The new method does not suffer the increased difficulties in mitigating the problematic sidelobe effects of an exscribed square.

3. Since the transform occurs prior to interpolation, the transform does not use data degraded by inexact interpolations. These interpolation errors are introduced later in the processing chain and lead to an overall lesser error.

4. Since the image usually contains fewer azimuth pixels than the number of original azimuth sample points, fewer interpolations are often required for the new technique.

5. Along with #3, the new technique does not require low pass filtering in conjunction with its interpolation as does the traditional method.

6. With the introduction of error later into the polar format processing chain, the post azimuth transform interpolation can potentially use lower-fidelity, smaller kernels than its traditional counterpart for the same image quality.

7. As a result of #4 and #6, fewer interpolations with smaller kernels allow greater efficiency, easier implementation, and faster operation.

3. Detailed Analysis

Recall that the more general model for the collected phase history data was adequately identified as

$$X_V(i,n) \approx A_R \sigma(s) \exp\, j\{k_x(i,n)s_x + k_y(i,n)s_y\} \qquad (20)$$

where,

$$k_x(i,n) = \frac{2}{c}\left[\omega_n + \gamma_n T_{s,n} i\right]\cos\psi_n \sin\alpha_n, \qquad (21)$$

$$k_y(i,n) = -\frac{2}{c}\left[\omega_n + \gamma_n T_{s,n} i\right]\cos\psi_n \cos\alpha_n \qquad (22)$$

Recall also that data ultimately needed to be placed on a grid that achieved for an integer index i'

$$\left[\omega_n + \gamma_n T_{s,n} i\right]\cos\psi_n \cos\alpha_n = \left[\omega_0 + \gamma_0 T_{s,0} i'\right]\cos\psi_0 . \qquad (23)$$

This is accomplished by forcing

$$\left[\omega_n + \gamma_n T_{s,n} i\right] = \left[\omega_0 + \gamma_0 T_{s,0} i'\right]\cdot\left(\frac{\cos\psi_0}{\cos\psi_n \cos\alpha_n}\right) \qquad (24)$$

or more specifically, can be implemented by adjusting

$$\omega_n = \omega_0 \cdot \left(\frac{\cos\psi_0}{\cos\psi_n \cos\alpha_n}\right) \text{ and } \gamma_n = \gamma_0 \cdot \left(\frac{\cos\psi_0}{\cos\psi_n \cos\alpha_n}\right) \qquad (25)$$

with $T_{s,n} = T_{s,0}$. Consequently, by allowing the waveform parameters to vary on a pulse-to-pulse basis, the range interpolation step is accomplished in the polar format algorithm [8]. Therefore, the radial wavenumber distance can be identified as:

$$k(i) = \frac{2}{c}\left[\omega_0 + \gamma_0 T_{s,0} i\right]\cdot\left(\frac{\cos\psi_0}{\cos\psi_n \cos\alpha_n}\right) \qquad (26)$$

As a result, if waveform parameters are adjusted this way, then $i = i'$. As with the conventional polar format algorithm, this also defines $k_x(i,n)$ as:

$$k_x(i,n) = k(i)\cos\psi_n \sin\alpha_n = \frac{2}{c}\left[\omega_o + \gamma_o T_{s,o} i\right]\cos\psi_0 \tan\alpha_n . \quad (27)$$

While it would be ideal to remove the dependence of k_x from index i with a similar real-time processing method, no such method currently exists. For this new method, it is however desirable to partially format the azimuth samples to achieve uniform sample spacing in the k_x direction. This can be accomplished by the radar emitting and collecting echo data at precise angles such that:

$$\tan\alpha_n = d\alpha \cdot n \quad (28)$$

Therefore, data is collected at wavenumber locations

$$k_x(i,n) = \frac{2}{c}\left[\omega_o + \gamma_o T_{s,o} i\right]\cos\psi_0 \cdot d\alpha \cdot n , \quad (29)$$

and for any ADC index value of i, the sample spacing is constant across n. This describes a trapezoidal aperture in Fourier space, and is illustrated in figure 7. This psuedo-polar grid data has a subtle difference from the original range interpolated polar wedge in that locations for k_x now exhibit a constant linear increment instead of a constant angular increment. That is, the expression for the phase history data becomes

$$X_V(i,n) \approx A_R \sigma(s) \exp j\left\{k_x(i,n)s_x + k_y(i)s_y\right\} \quad (30)$$

where the Fourier samples are located at

$$k_x(i,n) = \frac{2}{c}\left[\omega_0 + \gamma_0 T_{s,0} i\right]\cdot \cos\psi_0 \cdot d\alpha \cdot n, \quad (31)$$

$$k_y(i) = -\frac{2}{c}\left[\omega_0 + \gamma_0 T_{s,0} i\right]\cdot \cos\psi_0 \quad (32)$$

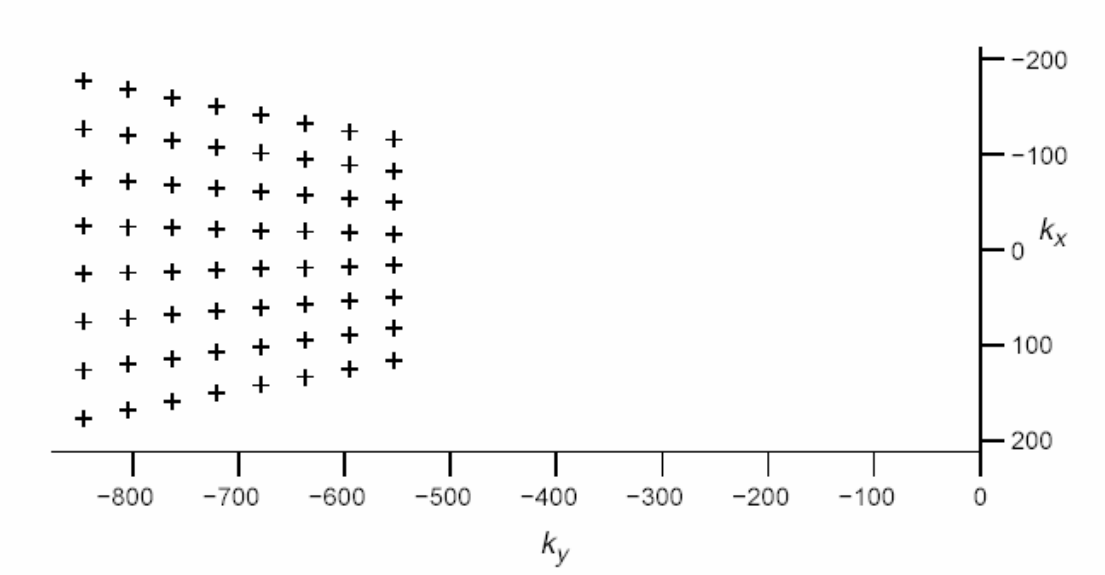

Figure 7: Trapezoidal locations of phase history data in Fourier space resulting from real-time adjustments in radar frequency, chirp rate, and pulse timing.

Completing the traditional polar format image formation is now simplified to a linear resampling in the azimuth direction and a 2-D FFT; or using separability, the total 2-D FFT operation can be broken into a 1-D azimuth FFT and a 1-D range FFT. For the new method however, the order of operations is changed. The total proposed image formation algorithm now becomes a 1-D azimuth FFT, followed by a linear resampling in the azimuth direction, and finally a 1-D range FFT. This process has a notable change from the traditional polar format image formation and that is the resampling in the azimuth direction is performed after the azimuth FFT. This option is available due to the linear spacing provided by the azimuth sampling of the phase history data. To show how the linear spacing in azimuth is significant, the frequency scaling property of the Fourier Transform is restated here as [11]:

$$\text{If} \qquad F\{y(t)\} = \int_{-\infty}^{\infty} y(t)\cdot e^{-j\cdot 2\pi\cdot f\cdot t}dt = Y(f), \tag{33}$$

$$\text{then} \qquad F\{y(a\cdot t)\} = \int_{-\infty}^{\infty} y(a\cdot t)\cdot e^{-j\cdot 2\pi\cdot f\cdot t}dt = \frac{1}{|a|}Y\left(\frac{f}{a}\right). \tag{34}$$

This also applies to the FFT as:

$$\text{If} \qquad FFT\left\{ y\left(\frac{n}{f_n}\right)\Big|_N \right\} = \sum_n y\left(\frac{n}{f_n}\right)\cdot e^{-j\frac{2\pi}{N}u\cdot n} = Y\left(\frac{f_n}{N}u\right), \text{ and} \tag{35}$$

$y\left(\frac{n}{f_n}\right)$ (length N sequence) is resampled to $y\left(\frac{n'}{f_n}\right) = y\left(\frac{a \cdot n}{f_n}\right)$ (length N' sequence),

$$\text{then} \quad FFT\left\{ y\left(\frac{n'}{f_n}\right)\Big|_{N'} \right\} = \sum_n y\left(a\frac{n}{f_n}\right) \cdot e^{-j\frac{2\pi}{N'}u \cdot n} = \frac{N}{N'} Y\left(\frac{f_n}{N}\frac{u}{a}\right). \qquad (36)$$

This allows that *for a given data set, performing a FFT and then linearly resampling the output, is equivalent to first linearly resampling the data set followed by a FFT*. That is, if linear resampling is involved, it can be done either before or after the FFT with a simple inversion of the frequency multiplication factor and a constant amplitude scaling.

Now, resuming the analysis of the formatted phase history data model, namely

$$X_V(i,n) \approx A_R \sigma(s) \exp j\{k_x(i,n)s_x + k_y(i)s_y\} \qquad (37)$$

where the Fourier samples are located at

$$k_x(i,n) = \frac{2}{c}\left[\omega_0 + \gamma_0 T_{s,0} i\right] \cdot \cos\psi_0 \cdot d\alpha \cdot n, \qquad (38)$$

$$k_y(i) = -\frac{2}{c}\left[\omega_0 + \gamma_0 T_{s,0} i\right] \cdot \cos\psi_0 \qquad (39)$$

the data can be rewritten as

$$X_V(i,n) \approx A_R \sigma(s) \exp j\{k_y(i)s_y\} \cdot \exp j\{k_x(i,n)s_x\}. \qquad (40)$$

Traditional polar format processing will at this point resample $k_x(i,n)$ in order to remove the dependence upon i. This is accomplished by interpolating such that

$$\left[\omega_o + \gamma_o T_{s,o} i\right] \cdot d\alpha \cdot n = \left[\omega_o\right] \cdot d\alpha \cdot n', \qquad (41)$$

or otherwise finding data values at locations

$$n = \frac{\left[\omega_o\right]}{\left[\omega_o + \gamma_o T_{s,o} i\right]} \cdot n' = \left(\frac{1}{1 + \frac{\gamma_o T_{s,o}}{\omega_o} i} \right) \cdot n'. \qquad (42)$$

The subsequent 1-D FFT's for image formation will then operate in the *n'* direction and the *i* direction. However, since the new method for image formation will be an azimuth transform prior to interpolation, we need to examine the 1-D FFT across index *n*. The 1-

D FFT along the *n* direction of the pre-formatted phase histories is described by the expression

$$FFT_n\left(X_V(i,n)\right)\approx$$

$$\sum_n\left[A_R\sigma(s)\exp j\{k_y(i)s_y\}\right]\cdot\exp j\{k_x(i,n)s_x\}\cdot\exp j\left\{\frac{-2\pi}{N}u\cdot n\right\} \qquad (43)$$

Consequently, the items contained in square brackets are constants as far as the transform is concerned, therefore

$$FFT_n\left(X_V(i,n)\right)\approx$$

$$\left[A_R\sigma(s)\exp j\{k_y(i)s_y\}\right]\cdot\sum_n\exp j\{k_x(i,n)s_x\}\cdot\exp j\left\{\frac{-2\pi}{N}u\cdot n\right\} \qquad (44)$$

Focusing on the summation and expanding k_x yields

$$\sum_n\exp j\left\{\frac{2}{c}\left[\omega_0+\gamma_0T_{s,0}i\right]\cdot\cos\psi_0\cdot d\alpha\cdot n\cdot s_x\right\}\cdot\exp j\left\{\frac{-2\pi}{N}u\cdot n\right\}. \qquad (45)$$

Combining the exponents in the summation yields

$$\sum_n\exp j\left\{\frac{2\cdot\omega_0\cdot\cos\psi_0}{c}\cdot d\alpha\cdot s_x\cdot\left(1+\frac{\gamma_0T_{s,0}}{\omega_0}i\right)-\frac{2\pi}{N}u\right\}\cdot n\,. \qquad (46)$$

Now, evaluating the sum results in

$$W_n\left(\frac{2\cdot\omega_0\cdot\cos\psi_0}{c}\cdot d\alpha\cdot s_x\cdot\left(1+\frac{\gamma_0T_{s,0}}{\omega_0}i\right)-\frac{2\pi}{N}u\right), \qquad (47)$$

making the FFT in azimuth

$$FFT_n\left(X_V(i,n)\right)\approx$$

$$\left[A_R\sigma(s)\exp j\{k_y(i)s_y\}\right]\cdot W_n\left(\frac{2\cdot\omega_0\cdot\cos\psi_0}{c}\cdot d\alpha\cdot s_x\cdot\left(1+\frac{\gamma_0T_{s,0}}{\omega_0}i\right)-\frac{2\pi}{N}u\right) \qquad (48)$$

where $W_n(\,)$ represents the image 'impulse response' or 'point spread function' in the azimuth direction. , We note that in the absence of any window functions or other data tapering

$$W_n(\Omega) = \sum_n e^{j\Omega n} \ , \tag{49}$$

which has the shape of a sinc( ) function near its peak value. The resultant FFT then has a peak response at

$$\frac{2\pi}{N} u = \frac{2 \cdot \omega_0 \cdot \cos\psi_0}{c} \cdot d\alpha \cdot s_x \cdot \left(1 + \frac{\gamma_0 T_{s,0}}{\omega_0} i\right) \tag{50}$$

Note that this response is still dependent on index *i*. To remove this dependence, we can define a new index u' such that

$$\frac{2\pi}{N} u' = \frac{2 \cdot \omega_0 \cdot \cos\psi_0}{c} \cdot d\alpha \cdot s_x . \tag{51}$$

and resample the data to interpolated positions where

$$u = \frac{\left[\omega_o + \gamma_o T_{s,o} i\right]}{\left[\omega_o\right]} \cdot u' = \left(1 + \frac{\gamma_o T_{s,o}}{\omega_o} i\right) \cdot u' . \tag{52}$$

As expected from the scaling property of the Fourier Transform, this is an inversion of the frequency multiplication factor for interpolation prior to the FFT (EQ. 42). Also, by interpolating in this manner, our data is no longer dependent upon index *i*. Specifically, we identify

$$FFT_n\left(X_V(i,n)\right) \approx$$

$$\left[A_R \sigma(s) \exp j\left\{k_y(i) s_y\right\}\right] \cdot W_n\left(\left(\frac{2 \cdot \omega_0 \cdot \cos\psi_0}{c} \cdot d\alpha \cdot s_x \cdot -\frac{2\pi}{N} \cdot u'\right)\left(1 + \frac{\gamma_o T_{s,o}}{\omega_o} i\right)\right) \tag{53}$$

and note that the index value *u*' for the location of the peak in W_n( ) no longer depends on index *i*. Although the index *i* sill resides within the argument of W_n( ), its impact is only an inconsequential modulation of the width of the impulse response, but not its more important location.

This means that after performing the azimuth FFT and subsequent interpolations, the data is only an inconsequential amplitude scale factor in difference from the traditional polar format interpolation prior to the FFT.

The image formation process then continues in the normal fashion with a range dimension FFT. Any residual blurring can then be addressed with conventional auto-focus operations in the usual manner.

Example SAR Image

Figure 8 shows a SAR image processed with this new polar format processing algorithm.

Figure 8: Image of bunkers generated in real-time with new polar format method. (Ku-band, 0.1 m resolution)

4. Conclusions

We have seen that the new proposed method of polar format image formation is equivalent to that of traditional polar format image formation in delivering MTRC compensated images. However, interpolation is never ideal and finite precision processing also leads to errors that are not present in the mathematical model. Therefore, there are several advantages to this new method of polar format image formation over traditional polar format image formation. These include:

1. By performing the FFT prior to resampling in the azimuth direction, all the frequency-space data is used. Traditional polar format processing typically uses data only within an inscribed rectangle in the polar wedge before performing a 2-D FFT for image formation. The width of the inscribed rectangle determines the azimuth resolution per each range index. As the range index increases, more of the polar wedge is excluded from the inscribed rectangle, thereby lowering the potential resolution in the azimuth direction. When the FFT is performed prior to azimuth interpolation, all of the frequency-space information is used and the post-interpolation is performed with the full available resolution. This will ultimately yield better results than using data only from an inscribed rectangular region, because the final azimuth resolution in this case is now limited by the performance of the interpolation filter.

2. Traditional techniques exist where the Fourier data is interpolated and zero-padded to create an exscribed rectangular data region. These techniques incur increased side lobe levels in the image. The new method of polar format image formation does not suffer the increased difficulties in mitigating the problematic side lobe effects of an exscribed rectangular data region.

3. The azimuth processing is done prior to any errors introduced by limited interpolation kernels. Ideal interpolation kernels are not realizable, and thus there are the tradeoffs between maintaining flat passbands, high transition slope, and good stopband rejection. With sampled data, frequencies above half the Nyquist rate are aliased back into the image. This creates unwanted errors that are unavoidable. On integer based processors like Field Programmable Gate Arrays (FPGA's), filter errors are compounded with quantization errors that accumulate by performing multiple operations (range interpolation, FFT's), the total error from traditional polar format processing can be larger than intended. By providing trapezoidal grid data directly, we reduce the number of errors introduced from range interpolation and the compounded quantization errors from the number of operations. By performing the azimuth FFT prior to interpolation, we further reduce the overall error, because the azimuth interpolation errors are introduced later in the processing chain.

4. Since the images usually contain fewer azimuth pixels than the number of original azimuth sample points, fewer interpolations are often required for the new technique and

this does not require low pass filtering in conjunction with its interpolation as does the traditional method.

5. With the introduction of error later into the polar format processing chain, the post azimuth transform interpolation can use lower-fidelity, smaller kernels in order to produce similar quality images to that of traditional polar format image formation. The advantage here is that interpolation will then require potentially fewer operations. Fewer interpolation operations can thus improve efficiency and ease of implementation without excessively degraded image quality.

The advantages in post azimuth transform interpolation make this new method of image formation better than traditional polar format image formation. The images produced offer the same or better quality. This new method also offers distinct advantages in overall efficiency due to the assistance of a real-time pre-formatting of the data and the potential to use smaller, lower fidelity interpolation kernels without large sacrifices in image quality. This new algorithm makes polar format processing even more viable in situations where it may not have been considered in the past and a good method when efficient, quality processing is necessary.

This page left intentionally blank.

References

[1] Brown, W.M., and R.J. Fredericks, “Range-Doppler Imaging with Motion though Resolution Cells,” IEEE Transactions on Aerospace and Electronic Systems, Vol. AES-5, No. 1, January 1969, pp 98-102.

[2] Walker, J.L., “Range-Doppler Imaging of Rotating Objects,” IEEE Transactions on Aerospace and Electronic Systems, Vol. AES-16, No. 1, January 1980, pp. 23-52.

[3] D.C. Munson, J.D. O’Brien, and W.K. Jenkins, “A Tomographic Formulation of Spotlight-Mode Synthetic Aperture Radar,” Proc. IEEE, vol. 74, pp. 1165-1166, Aug. 1986.

[4] W. J. Caputi Jr., "Stretch: A Time-Transformation Technique", IEEE Transactions on Aerospace and Electronic Systems, Vol. AES-7, No. 2, pp 269-278, March 1971

[5] C. V. Jakowatz Jr., D. E. Wahl, P. H. Eichel, D. C. Ghiglia, P. A. Thompson, *Spotlight-Mode Synthetic Aperture Radar: A Signal Processing Approach*, ISBN 0-7923-9677-4, Kluwer Academic Publishers, 1996.

[6] Walter G. Carrara, Ron S. Goodman, Ronald M. Majewski, *Spotlight Synthetic Aperture Radar, Signal Processing Algorithms*, ISBN 0-89006-728-7, Artech House Publishers, 1995.

[7] Bryan L. Burns, J. Thomas Cordaro, “Imaging Synthetic Aperture Radar”, US Patent No. 5,608,404, March 4, 1997

[8] Armin W. Doerry, *Synthetic Aperture Radar Processing with Tiered Subapertures*, Ph.D. Dissertation, The University of New Mexico, Albuquerque, New Mexico, May 1995.

[9] Wayne Lawton, “A New Polar Fourier Transform for Computer-Aided Tomography and Spotlight Synthetic Aperture Radar,” IEEE Transactions on Acoustics, Speech, and Signal Processing, Vol. 36, No. 6, pp. 931-933, June 1988.

[10] B. L. Burns, J. T. Cordaro, “SAR image formation algorithm that compensates for the spatially variant effects of antenna motion”, SPIE Proceedings, Vol 2230, SPIE’s International Symposium on Optical Engineering in Aerospace Sensing, Orlando, 4-8 April 1994.

[11] Alan V. Oppenheim, Ronald W. Schafer, *Digital Signal Processing*, Prentice-Hall (1975).

[12] Armin W. Doerry, “Real-time Polar-Format Processing for Sandia’s Testbed Radar Systems”, Sandia National Laboratories Report SAND2001-1644P, June 2001.

DISTRIBUTION

Unlimited Release

1	MS 0509	M. W. Callahan	5300
1	MS 0529	B. L. Remund	5340
1	MS 0519	B. L. Burns	5340
1	MS 0503	T. J. Mirabal	5341
1	MS 0519	W. H. Hensley	5342
1	MS 0519	T. P. Bielek	5342
1	MS 1330	A. W. Doerry	5342
1	MS 0519	D. Harmony	5342
1	MS 0519	J. A. Hollowell	5342
1	MS 0529	S. S. Kawka	5342
1	MS 0519	M. S. Murray	5342
1	MS 0519	B. G. Rush	5342
1	MS 0519	D. G. Thompson	5342
1	MS 1330	K. W. Sorensen	5345
1	MS 1330	J. Bach	5345
1	MS 0529	B. C. Brock	5345
1	MS 1330	D. F. Dubbert	5345
1	MS 1330	G. R. Sloan	5345
1	MS 1330	S. M. Becker	5348
1	MS 0519	S. M. Devonshire	5348
1	MS 1330	M. W. Holzrichter	5348
1	MS 1330	O. M. Jeromin	5348
1	MS 1330	G. D. Martin	5348
1	MS 0519	B. E. Mills	2348
1	MS 1330	P. G. Ortiz	5348
1	MS 1330	D. C. Sprauer	5348
1	MS 1330	A. D. Sweet	5348
1	MS 0519	M. E. Thompson	5348
1	MS 0519	L. M. Wells	5354
1	MS 0519	D. L. Bickel	5354
1	MS 0519	J. T. Cordaro	5354
1	MS 0519	J. DeLaurentis	5354
1	MS 1330	A. E. Mihalik	5354
1	MS 0311	F. M. Dickey	2616
2	MS 0899	Technical Library	4536